

Multi-scale Transport Simulation of Internal Transport Barrier Formation and Collapse

S Tokunaga 1), M Yagi 2), S-I Itoh 2), K Itoh 3)

1) Interdisciplinary Graduate School of Engineering Sciences, Kyushu University, Kasuga, Fukuoka, 816-8580, Japan

2) Research Institute for Applied Mechanics, Kasuga, Fukuoka, 816-8580, Japan

3) National Institute for Fusion Science, National Institute of Natural Sciences, Toki, Gifu, 509-5292, Japan

e-mail contact of main author: toku@riam.kyushu-u.ac.jp

Abstract. The mechanism of internal transport barrier (ITB) collapse in the reversed magnetic shear configuration is investigated using a global Ion Temperature Gradient driven drift wave (ITG) turbulence code. The heating source and the Toroidal Momentum Source (TMS) is introduced to follow the self-consistent evolution of the ion temperature and flow profiles. The Toroidal Flow Shear (TFS) effect on the dynamics of ITB evolution is clarified. It is found that the lifetime of ITB depends on the total flow shear, i.e., the equilibrium flow shear determined by TMS and the ITG turbulence driven flow shear.

1. Introduction

Internal Transport Barrier (ITB) has been observed in many tokamaks with a reversed magnetic shear configuration [1]. ITB is expected to be beneficial for the steady state operation of ITER. The improved performance by ITB was surveyed in multi-machine comparisons [2]. So far much works on ITB formations have been done theoretically and numerically [3, 4, 5]. The velocity shear and the negative magnetic shear as well as the zonal flow (ZF) play an important role for ITB formation [6]. Recently, the turbulence spreading is examined for the barrier propagation in ITG turbulence[7]. The turbulent spreading can allow turbulence to penetrate the regions where local analysis predicts low level of transport [8]. Moreover, turbulent spreading can dynamically couple different regimes of plasma such as the edge and core, so that it gives rise to the non-local effects. The non-locality of the plasma transport is observed in many tokamaks such as the temperature profile stiffness [9, 10] and the rapid heat pulse propagation from the edge to the core [11, 12]. To understand such non-locality of the transport property, it is necessary to perform the global multi-scale simulation including the profile modification effect, non-local interaction between the meso-scale structures.

In addition to explore the multi-scale interaction between turbulence and transport, the control of ITB is another important issue for ITER operation. Neutral Beam Injection (NBI) is used to optimize the confinement of the tokamak plasma and to develop the steady state operation technique, such as dynamical current profile control, the sawtooth oscillation control by off-axis injection and so on [13, 14, 15, 16, 17].

In this paper, we investigate the multi-scale interaction between ITG turbulence and transport in terms of ITB formation and collapse. Introducing the heating source and TMS, the self-consistent evolution of the ion temperature and flow profiles is followed. The TFS effect on the dynamics of ITB evolution is clarified. It is found that the lifetime of ITB depends on the

toroidal flow shear, i.e., the equilibrium flow shear determined by TMS and the ITG turbulence driven flow shear.

2. Numerical Model

2.1. Model Equations

We employ the simplified version of the “3+1” gyro-fluid model [18] proposed by Ottaviani *et al.* [19] and modified by Yagi [7] to investigate the ITG turbulence transport by global simulation. The set of equations consists of the ion density, the ion parallel momentum and the ion temperature evolution equations :

Ion density equation :

$$\frac{dW}{dt} + \kappa_n \frac{1}{r} \frac{\partial \Phi}{\partial \vartheta} + A \nabla_{\parallel} V = \varepsilon \hat{\omega}_d F + \rho_* \frac{q}{\varepsilon} \mu^{\text{NC}} \frac{1}{r} \frac{\partial (r U_p)}{\partial r} - \rho_*^2 \mu \nabla_{\perp}^4 F. \quad (1)$$

Ion parallel momentum equation :

$$\frac{dV}{dt} = -A \nabla_{\parallel} F + 4\mu \nabla_{\perp}^2 V - \mu^{\text{NC}} U_p - A \sqrt{\frac{1}{\tau} \frac{2}{5}} \sqrt{\pi} |k_{\parallel}| V + \frac{2}{5} A \frac{1}{\tau} \nabla_{\parallel} T + S V_{pl} \quad (2)$$

Ion temperature evolution equation :

$$\frac{3}{2} \left(\frac{dT}{dt} + \kappa_T \frac{1}{r} \frac{\partial \Phi}{\partial \vartheta} \right) - \left(\frac{dn}{dt} + \kappa_n \frac{1}{r} \frac{\partial \Phi}{\partial \vartheta} \right) = -\frac{9}{5 \sqrt{\pi}} \sqrt{\frac{1}{\tau}} A |\nabla_{\parallel}| T + \frac{2}{5} A \nabla_{\parallel} V + \chi_{\perp} \nabla_{\perp}^2 T + S T_i, \quad (3)$$

where, $W = n - \nabla_{\perp}^2 F$ is the generalized vorticity, $n = \Phi - \langle \Phi \rangle$ is the fluctuating density, $F = \Phi + p/\tau$ is the generalized potential with $\tau \equiv T_{e0}/T_{i0}$, $p = n + T$ is the fluctuating ion pressure and $\langle \Phi \rangle$ is the flux surface averaged potential, which is equivalent to $\Phi_{m=0, n=0}$ in Fourier space. The approximation $p_1 = T_{i0}(r_s)n_1 + n_0(r_s)T_{i1}$ is made where $r_s = 0.6$ indicates the location of the q_{min} surface. $U_p = V + \rho_* \frac{q}{\varepsilon} \frac{\partial F}{\partial r}$ represents the poloidal velocity, $\kappa_T = -d \ln T_0 / dr$ and $\kappa_n = -d \ln n_0 / dr$ indicate the inverse of the gradient scale length of the ion temperature and density, respectively, $\hat{\omega}_d = 2 \cos \vartheta \frac{1}{r} \frac{\partial}{\partial \vartheta} + 2 \sin \vartheta \frac{\partial}{\partial r}$ is the curvature operator, $A = \varepsilon_a / \rho_*$ is the ratio of the inverse aspect ratio $\varepsilon_a = a/R_0$ and the normalized ion gyro-radius measured by the electron temperature $\rho_* = \rho_s/a$. We also introduced $\varepsilon = r/R_0$ as the local inverse aspect ratio. The transport coefficients are given by the ion thermal diffusivity χ , the neoclassical ion viscosity μ^{NC} and the ion viscosity μ . Ion Landau damping is also taken into account as a collisionless dissipation [20]. The normalization : $t/t_B \rightarrow t$, $r/a \rightarrow r$, $z/R_0 \rightarrow z$, $e\Phi/T_{e0} \rightarrow \Phi$, $V/c_s \rightarrow V$, $T/T_{i0} \rightarrow T$, $\chi/(\rho_s c_s) \rightarrow \chi$, $\mu/(m_i n_0 \rho_s c_s) \rightarrow \mu$, $\mu^{\text{NC}} a^2 / (\rho_s c_s) \rightarrow \mu^{\text{NC}}$ is used for the system, where $t_B = a^2 / \chi_B$ represents the Bohm time determined by the Bohm diffusion $\chi_B = cT_{e0}/(eB)$.

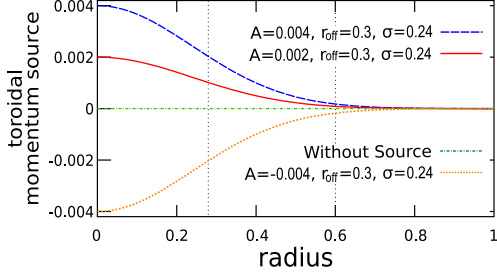


FIG. 1. Radial profiles of toroidal momentum source.

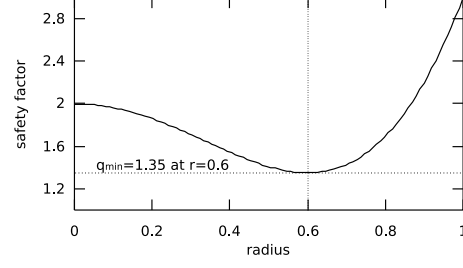


FIG. 2. Safety factor q profile with reversed magnetic shear.

2.2. Source Terms and Initial Conditions

The Gaussian type toroidal momentum source is introduced in eq.(2) to investigate the effect of the equilibrium toroidal flow on ITB sustainment :

$$S V_{pl}(r) = A \exp \left[-\frac{(r - r_{off})^2}{2\sigma^2} \right]. \quad (4)$$

We examined four cases 1) without TMS, 2) with small TMS : $A = 2 \times 10^{-3}$, $r_{off} = 0$ and $\sigma = 0.24$, 3) with large TMS : $A = 4 \times 10^{-3}$, $r_{off} = 0$ and $\sigma = 0.24$ and 4) with large negative TMS : $A = -4 \times 10^{-3}$, $r_{off} = 0$ and $\sigma = 0.24$. FIG. 1 shows the momentum source profiles for the cases 2) 3) and 4). The positive and negative sign of the TMSs correspond to the co-directional and counter-directional momentum input along the toroidal magnetic field respectively. They produce toroidal ion flow velocity profile whose max value is about 10% ~ 20% of ion sound velocity and the absolute value of the toroidal flow shear takes a peak value at $r \sim 0.28$ at $t \sim 60$.

A heat source term is also introduced in eq. (3). It is given by

$$S T_i(r) = -4 \times 10^{-3} \frac{(2r^2 - 1)^2}{(1 - r_s^2)^2}, \quad (5)$$

with $r_s = 0.6$. This source gives an ion temperature profile $T_i(r) = (1 - r^2)^2 / (1 - r_s^2)^2$ if the relation : $\chi_{\perp}(1/r)d/dr(rdT/dr) + S T_i = 0$ is held. In our model, the ion temperature can not be divided into equilibrium and fluctuating quantities such as $T = T_0 + \tilde{T}$, but is rather solved as a whole.

For the safety factor q profile, we employ reversed magnetic shear profile, proposed by Garbet *et al.* [21], which is given by $q(r) = q_{\min} + C_2(r^2 - r_s)^2 + C_3(r^2 - r_s^2)^3$, with $q_{\min} = 1.35$, $r_s = 0.6$, $C_2 = 4.66$, and $C_3 = -0.987$. Note that the (m,n)=(4,3) mode is off-resonant in this configuration as is shown in FIG. 2.

The equilibrium density profile is given by $n_0(r) = (1 - r^2)/(1 - r_s^2)$ which is fixed during the simulation due to the constraint that no particle flux is generated in the system: $n = \Phi - \langle \Phi \rangle$.

3. Results and Discussions

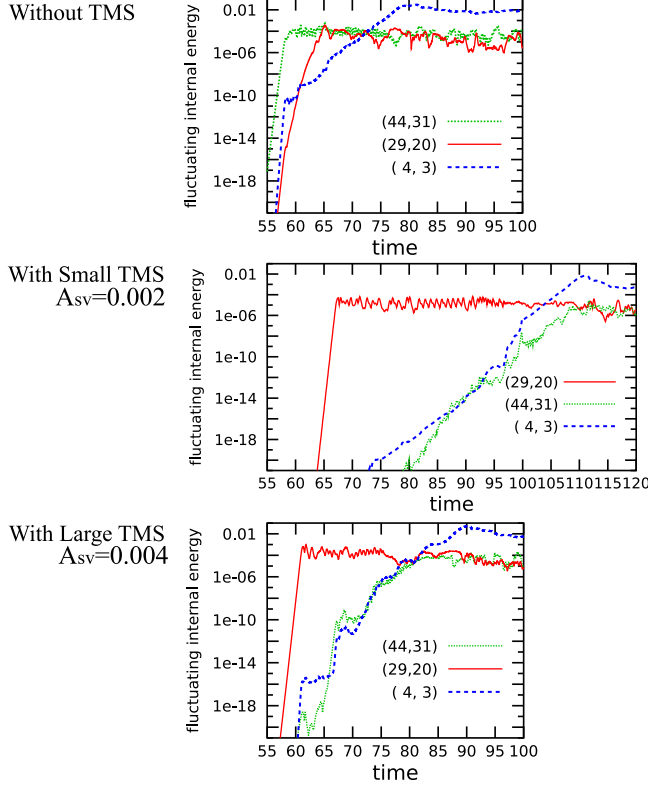


FIG. 3. Left: Time evolutions of fluctuating internal energies in cases : (1) without TMS (top), (2) with small TMS (middle) and (3) with strong TMS (bottom), respectively .

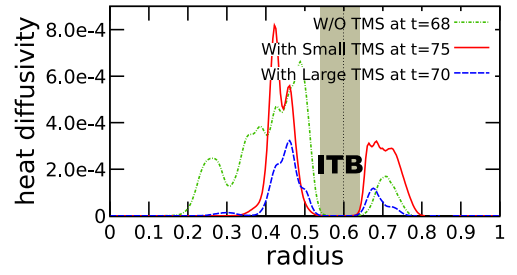


FIG. 4. Snapshots of heat transport coefficient radial profile where ITB exists in shaded region.

3.1. ITB Formation and Collapse

FIG. 3 shows temporal evolution of the fluctuating internal energy of (44,31), (29,20) and (4,3) modes. In the simulation, the ion temperature develops according to the heating source. When the temperature gradient exceeds the threshold of the ITG instability, it is destabilized and begins to grow. In the case without TMS, the (44,31), (45,31) etc. are destabilized at $t \sim 52$ on these resonant surfaces which are located on $r \sim 0.4$ and saturate at $t \sim 58$. On the other hand, in the cases with TMS, the (29,20) mode is destabilized at first. In the case with small TMS, it is destabilized at $t \sim 60$ and saturates at $t \sim 67$. In the case with large TMS, it is destabilized at $t \sim 55$ and saturates at $t \sim 61$. The saturation level is almost same for three cases, i.e., $\sim 10^{-5}$.

After the saturation of ITG modes, the internal transport barrier forms in vicinity of the q_{min} ($0.55 < r < 0.65$) in each case (FIG. 4). The shaded region indicates ITB region where the turbulence is suppressed across the q_{min} . It is clearly shown that the turbulent transport around

FIG. 5. The (4,3) mode exceeds the zonal component, then the ITB collapses. In the test simulation omitting the flow energy of (4,3) mode on each calculation step, ITB remains beyond $t = 150$.

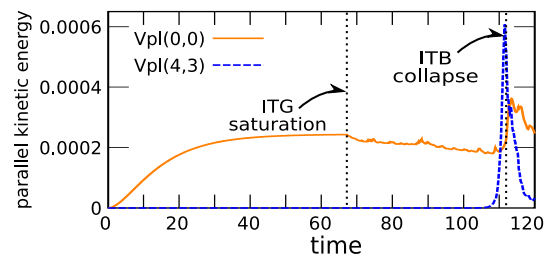
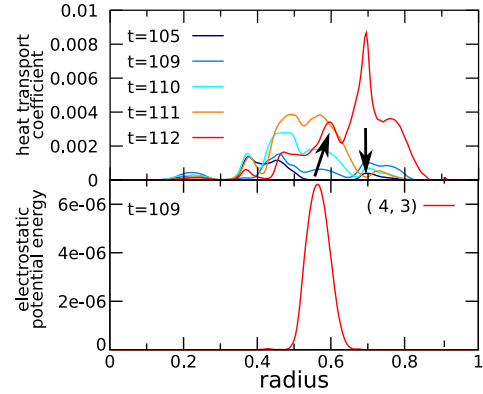


FIG. 6. (Top) Time slices of the radial profile of heat transport coefficient during the collapse phase of ITB. Transport starts to rise from $t = 105$ in $r \sim 0.55$. Until $t = 111$, transport is suppressed at $r = 0.7$. Consequently, it causes the concentration of the temperature gradient into $r \sim 0.7$. At $t = 112$, the ITB completely collapses abruptly.

(Bottom) Radial profile of the (4,3) component of electrostatic potential energy at $t = 109$. The gradual arise of transport in this phase seems to be due to the growth of the (4,3) mode.



$r \sim 0.3$ is reduced in the cases with TMS. There is no essential difference among them on the ITB location. However, the quantitative difference is observed on the life time of the ITB. FIG. 5 indicates the temporal evolution of parallel ion kinetic energy of the (0,0) and (4,3) modes in the case with small TMS. The (4,3) mode grows exponentially and exceeds zonal component at $t \sim 110$. Then the ITB starts to collapse and finally the heat energy stored inside of ITB bursts away at $t = 112$. This phenomena is common in each case.

FIG. 6 shows the time slices of turbulent thermal conductivity. ITB begins to collapse from the inside gradually from $t = 105$. The electrostatic potential energy of (4,3) mode which is shown in the bottom of FIG. 6 contributes the transport in the region $0.5 < r < 0.65$ and causes the steepening of the temperature gradient at $r \sim 0.7$. When the gradient exceeds the threshold, ITG modes are excited at $r = 0.7$. These simultaneously produce the zonal flow outside edge of the ITB. At $t = 112$, the ITB cannot be sustained any more, then the energy burst takes place.

In the simulation in which the flow energy of the (4,3) mode is thrown away on each time step, we confirmed that the ITB collapse does not occur at least until $t = 150$ even in the case without TMS. This mode is chosen by the system, since the $q_{min} = 1.35$ is near to the $4/3 = 1.33 \dots$.

FIG. 7 shows time evolution of the fluctuating internal energy in the case with negative TMS. In this case, the (45,31), (44,31) etc. are destabilized at first. The turbulent transport around $r \sim 0.3$ is not suppressed. The ITB collapse begins at $t \sim 67$ and bursts away at $t \sim 76$. The counter-directional momentum input does not contribute to the enhancement of the lifetime of the ITB in this case.

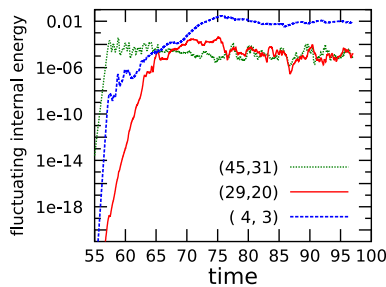


FIG. 7. Time evolution of fluctuating internal energies in the case with counter-directional TMS.

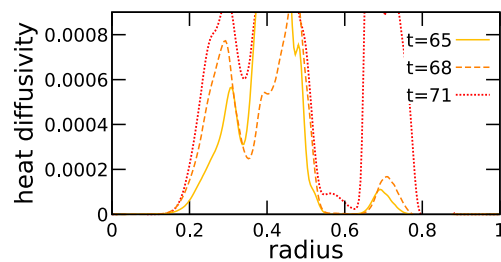


FIG. 8. Snapshots of heat transport coefficient radial profile in the case with counter-directional TMS.

3.2. Toroidal flow shear effect on meso-scale structure

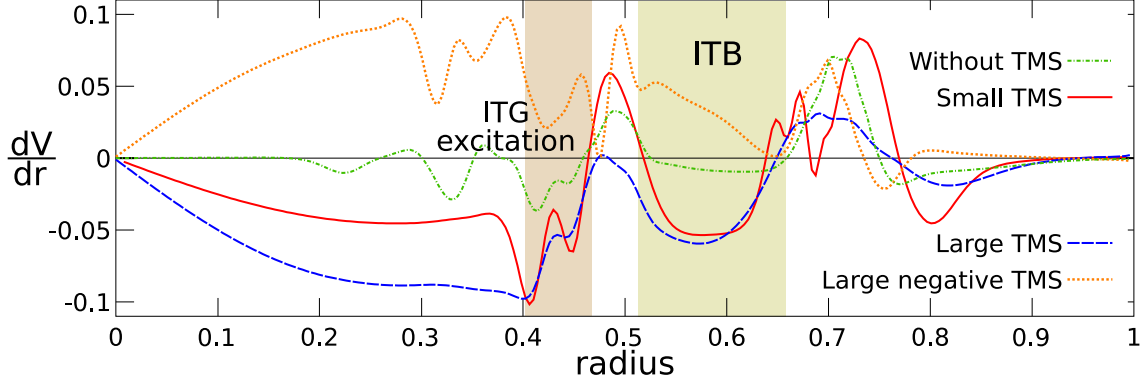


FIG. 9. Typical radial profiles of toroidal flow shear at, 1) $t = 75$ with small TMS, 2) $t = 70$ with large TMS, 3) $t = 65$ with large negative TMS and 4) $t = 68$ without TMS.

FIG.9 shows the typical radial profiles of the toroidal flow shear in the phase of ITB sustainment. The corresponding turbulent heat diffusivities are shown in FIG.4 and 8. In all cases, a strong velocity shear forms around $r \sim 0.7$, which sustain ITB foot. The main difference between small TMS case and other cases is that the velocity shear is almost zero at $r \sim 0.47$ except small TMS case. This position gives the boundary between ITG unstable region and ITB region. In the case with large TMS, there is a tendency that the flow shear determined by TMS is cancelled with that generated by ITG turbulence at $r \sim 0.47$. The similar tendency is observed for the case with large negative TMS. Next, we investigate the energy transfer channels to the (4,3) mode in the case with small TMS. FIG.10 and 11 shows energy transfer to the (4,3) mode at $t = 85$ (in the phase of ITB sustainment) and $t = 106$ (in the early phase of ITB collapse). The red bar indicates the energy transfer to the (4,3) mode from the other mode and the blue bar the energy transfer to the other mode from the (4,3) mode, where the energy channel satisfies the relation : $m_1 + m_2 = 4$, $n_1 + n_2 = 3$. $m_1 = 0$ indicates the energy channel from (0,0)-(4,3), i.e., quasi-linear channel. $m_1 = 3, 5$ indicates that from the toroidal coupling. The band $30 < m_1 < 40$ corresponds to ITG modes. We may call the modes $5 < m_1 < 30$ as mediators, which have relatively broad radial eigen-function. They are excited by non-linear coupling among ITG modes, then the coupling among mediators generates (4,3) mode. It is

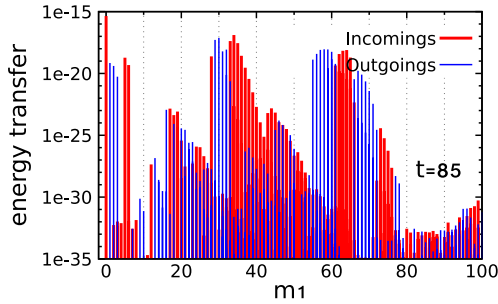


FIG. 10. Energy transfer to the (4,3) mode via three wave coupling at $t = 85$. Horizontal axis indicates the poloidal mode number which satisfies the relation: $m_1 + m_2 = 4$ and $n_1 + n_2 = 3$.

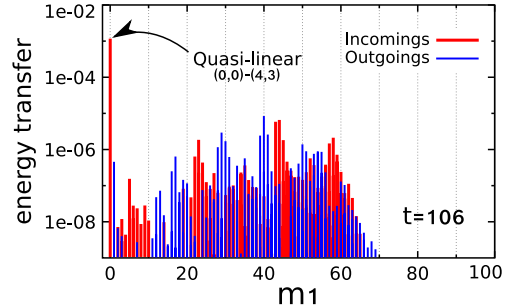


FIG. 11. Energy transfer to the (4,3) mode via three wave coupling at $t = 106$.

confirmed that only quasi-linear channel to the (4,3) mode can lead to the ITB collapse but the life time of ITB extends to $\Delta t \sim 5$ by the simulation where all channels to the (4,3) mode except the quasi-linear channel are closed. The sustainment of ITB depends on the excitation of the (4,3) mode and the stabilization of ITG modes at $r \sim 0.47$ and $r \sim 0.7$. How the total flow shear should be determined is not resolved, especially the negative TMS. This is an open question and left for a future work.

4. Conclusion

We investigated ITB formation and collapse with reversed magnetic shear configuration using the multi-scale global transport simulation code based on the gyro-fluid model. Heat source term and toroidal momentum source term are introduced to study the effect of toroidal flow shear on the ITB dynamics. Collapse of the ITB in this simulation starts without trigger. It can be understood as a kind of global relaxation. A meso-scale mode locate in vicinity of q_{min} plays important role for this global relaxation process. The notable enhancement of the ITB sustainment time was observed with the toroidal momentum source whose amplitude is rather small. It was explained by the flow shear stabilization of ITG turbulence. The rather small positive (co-directional) momentum input produced the effective flow shear inside ITB region, which consists of mean flow shear and turbulence generated flow shear. The extension of the ITB lifetime by negative momentum input was not observed in this simulation. It is also found that the quasi-linear effect due to the temperature profile modification is quite important, especially in the final collapse phase, quasi-linear effect plays a dominant role.

References

- [1] KOIDE, Y., et. al., "Internal transport barrier on $q=3$ surface and poloidal plasma spin up in JT-60U high β_p discharges.", Phys. Rev. Lett. **4** (1978) 3662.
- [2] LITAUDON, X., et. al., "Status and prospects for advanced tokamak regimes from multi-machine comparisons using the 'Internal Tokamak Physics Activity' database", Plasma Phys. Control. Fusion **46** (2004) A19.
- [3] ITOH, K. and ITOH, S.-I., "Transient response of transport at transport barrier formation", Plasma Phys. Control. Fusion **44** (2002) 367.
- [4] KISHIMOTO, Y., et. al., "Toroidal mode structure in weak reversed magnetic shear plasma and its role in the internal transport barrier", Plasma Phys. Control. Fusion **41** (1999) A663.
- [5] CANDY, J., et. al., "Smoothness of turbulent transport across a minimum- q surface", Phys. Plasmas **11** (2004) 1879.
- [6] DIAMOND, P. H., et. al., "Zonal flows in plasma - A review". Plasma Phys. Control. Fusion **47** (2005) R35.
- [7] YAGI, M., et. al., "Turbulence spreading in reversed shear plasmas", Plasma Phys. Control. Fusion **48** (2006) A409.
- [8] DIMITS, A. M., et. al., "Simulation of ion temperature gradient turbulence in tokamaks", Nucl. Fusion **40** (2000) 661.
- [9] HORTON, L. D., et. al., "Performance near operational boundaries", Plasma Phys. Control. Fusion **41** (1999) B329.
- [10] URANO, H., et. al., "Edge-core relationship of ELMy Hmode plasmas in JT-60U", Plasma Phys. Control. Fusion **44** (2002) A437.

- [11] GENTLE, K. W., et. al., “Strong Nonlocal Effects in a Tokamak Perturbative Transport Experiment”, *Phys. Rev. Lett.* **74** (1995) 3620.
- [12] RYTER, F., et. al., “Propagation of cold pulses and heat pulses in ASDEX Upgrade”, *Nucl. Fusion* **40** (2000) 1917.
- [13] SHIRAI, H., et.al., “Reduced transport and E_r shearing in improved confinement regimes in JT-60U”, *Nucl. Fusion* **39** (1999) 1713.
- [14] SAKAMOTO, Y., et. al., “Characteristics of internal transport barriers in JT-60U reversed shear plasmas”, *Nucl. Fusion* **41** (2001) 865.
- [15] SUZUKI, T., et. al., “Off-axis current drive and real-time control of current profile in JT-60U”, *Nucl. Fusion* **48** (2008) 045002.
- [16] CHAPMAN, I. T., et. al., “Sawtooth control using off-axis NBI”, *Plasma Phys. Control. Fusion* **50** (2008) 045006.00
- [17] CONNOR, J. W., et. al., “A review of internal transport barrier physics for steady-state operation of tokamaks”, *Nucl. Fusion* **44** (2004) R1.
- [18] BEER, M. A. and HAMMETT, G. W., “Toroidal gyrofluid equations for simulations of tokamak turbulence”, *Phys. Plasmas* **3** (1996) 4046.
- [19] OTTAVIANI, M. and MANFREDI, G., “The gyro-radius scaling of ion thermal transport from global numerical simulations of ion temperature gradient driven turbulence”, *Phys. Plasmas* **6** (1999) 3267.
- [20] CHANG, Z. and CALLEN, J. D., “Unified fluid/kinetic description of plasma microinstabilities. Part I: Basic equations in a sheared slab geometry”, *Phys. Fluids B* **4** (1992) 1167.
- [21] GARBET, X., et. al., “Global simulations of ion turbulence with magnetic shear reversal”, *Phys. Plasmas* **8** (2001) 2793.
- [22] GARBET, X., “Turbulence in fusion plasmas: key issues and impact on transport modelling”, *Plasma Phys. Control. Fusion* **43** (2001) A251.
- [23] ZASTROW, K.-D., et. al., “Transfer rates of toroidal angular momentum during neutral beam injection”, *Nucl. Fusion* **38** (1998) 257.